Revista Minelor – Mining Revue
ISSN-L 1220-2053 / ISSN 2247-8590
vol. 32, issue 1 / 2026, pp. 34-54

EXPERIMENTAL RHEOLOGICAL CHARACTERIZATION AND VISCOUS-PLASTIC BEHAVIOR MODELLING OF ROCK SALT FROM SLĂNIC PRAHOVA UNDER UNIAXIAL LOADING

Mihaela TODERAȘ[1*]

[1] University of Petrosani, Petroșani, Romania, toderasmihaela@yahoo.com

DOI: 10.2478/minrv-2026-0004
received – 15.01.2026 / revised – 19.01.2026
accepted – 16.02.2026 / published – 24.03.2026

Abstract: *The time-dependent behaviour specific to geological formations, known as creep, was investigated through a series of multi-stage uniaxial creep tests, applying six increasing stress increments until reaching the failure stage. The analysis confirmed the presence of the three distinct creep stages: primary, secondary (steady-state or stationary), and tertiary. Based on the strain-time data, it was demonstrated that the relationship between the ultimate axial strain (ε_f) and the final time (t_f) aligns with a power-law model. For modelling secondary creep, Norton's power law was applied, yielding a stress exponent of $n \approx 1.57$ and $\ln(C) \approx -10.74$. This relatively low exponent value suggests that diffusion-based creep mechanisms may be dominant. However, the magnitude and non-monotonic variation of the secondary creep rate with respect to stress indicate the limitations of this simplified model, highlighting the microstructural complexity of the salt. In the tertiary creep stage, under the highest applied load (117.6 daN/cm^2), a pronounced acceleration of the strain rate was observed. Exponential extrapolation of this phase led to an estimated service life of approximately 123 days before reaching a critical strain of 5 %. The results are significant for calibrating constitutive damage models and for forecasting the long-term stability and lifespan of underground structures within Slănic Prahova salt deposit.*

Keywords: *rock salt, secondary creep, tertiary creep, Norton's law, viscous-plastic behaviour, diffusion*

1. Introduction

The geomechanical behaviour of rocks represents a fundamental field of study for ensuring stability and safety across numerous engineering applications, ranging from mining operations to underground repositories and civil constructions [1, 2, 3, 4]. Among geological formations, rock salt occupies a distinct position due to its pronounced viscous-plastic properties, which result in time-dependent behaviour known as creep [5, 6, 7, 8]. This phenomenon involves the slow, continuous deformation of the material under constant loads, even at stress levels below the yield strength, and is particularly relevant for salt massifs subjected to long-term loading.

Rock salt hold strategic significance in underground engineering owing to their specific physical properties, which include effective impermeability and relatively high thermal conductivity [9, 10, 11].

From a mechanical perspective, their defining characteristic is a dominant viscous-plastic behaviour [9], [12, 13]. Under the influence of in situ stress and temperature [14, 15], this behaviour manifests as creep—a progressive, time-dependent deformation that evolves even under constant loading [16, 17]. This capacity for controlled plastic deformation grants the salt massif a tendency to gradually reduce or eliminate internal structural discontinuities, such as microfractures and voids, over time and under stress [18, 19, 20, 21].

This process occurs through several primary physical mechanisms: plastic deformation, diffusion, and recrystallization. Plastic deformation (creep) describes the state in which salt deforms slowly under a constant load (or lithostatic stress). This deformation leads to the progressive closure of pores and open fissures; the salt mass surrounding a discontinuity migrates slowly, infilling the void [22, 23, 24].

[*] Corresponding author: Toderaș Mihaela, prof. Ph.D. eng., University of Petrosani, Petrosani, Romania, Contact details: University of Petrosani, 20 University Street, toderasmihaela@yahoo.com

 vol. 32, issue 1 / 2026
pp. 34-54

Diffusion-based creep mechanisms (such as, grain-boundary diffusion) enable the transport of sodium and chloride ions (Na+ and Cl-) toward fracture surfaces. This transport facilitates the welding and consolidation of fracture walls upon contact, thereby restoring the rock's structural integrity [21, 22]. At the microscopic level, stress-induced recrystallization can lead to the formation of new mineral bonds across fractured surfaces [25].

This property or capacity for the gradual elimination of structural discontinuities has major implications for engineering design because it contributes to the long-term stability of caverns and underground rooms, as the salt massif can partially restore its strength after being affected by the excavation process (Excavation Damaged Zone or EDZ). By closing fractures and leakage pathways, salt maintains and even enhances its impermeability [26, 27, 28]. This is essential for radioactive waste repositories or gas storage reservoirs, where fluid migration must be strictly prevented. While advantageous, this phenomenon must be incorporated into advanced constitutive models to accurately predict salt behaviour over decades or centuries [29, 30, 31].

In brief, the tendency toward the gradual elimination of structural discontinuities is the intrinsic capacity of salt for structural consolidation through viscous-plastic deformation—a critical process that ensures the safety and stability of underground structures.

Conversely, this same phenomenon imposes the critical challenge of excavation closure, potentially compromising the long-term stability and operational lifespan of engineered structures (mines, repositories, storage reservoirs). Given this duality, underground structures within salt massifs (such as those at Slănic Prahova) necessitate the development and calibration of precise predictive models. The Slănic Prahova salt deposit from Romania constitutes an essential case study [32]. The specific rheological characterization of this material is indispensable, as constitutive parameters—such as the creep exponent (n) from Norton's law or the long-term strength (σ_{lld})—are strongly influenced by variations in mineralogical composition, impurities, and the granular structure of the salt. A quantitative understanding of these parameters provides the foundation for evaluating the safety of engineering works [32].

A review of the specialized literature [7, 8, 13, 21, 22] confirms that creep is governed by three distinct stages (primary, secondary, and tertiary), and modelling efforts have focused on accurately capturing these transitions [33]. Regarding classical models (Norton, Cristescu), the early studies by Griggs [34] and Stamatiu [35, 36] established the theoretical foundations of creep. Norton's Law ($\dot{\varepsilon}\ \alpha\ \sigma^n$) remains the empirical reference form for secondary creep. Subsequently, advanced models, such as the elastic/viscous-plastic frameworks developed by Cristescu [37] and Jin & Cristescu [38], have enabled the phenomenological description of both stages (transient and steady-state), providing a robust basis for numerical engineering analyses. Modern research in salt rheology transcends the simple application of empirical models, focusing instead on elucidating the microscopic mechanisms responsible for macroscopic deformation and modelling the damage phenomena that govern the advanced stages of creep. A major trend in recent literature aims to establish a direct correlation between constitutive model parametrization and the dominant physical creep mechanism.

In this context, the stress exponent (n) from Norton's Law plays a central role. Its numerical value is essential for identifying the active deformation mechanism: a value of around 1 or 2 generally indicates diffusion-based mechanisms (for example, Nabarro-Herring or Coble creep), while higher values, typically between 3 and 5, suggest a dominance of mechanisms controlled by dislocation glide and climb. Understanding this value is important for predicting the long-term behaviour of salt [35, 37].

Another critical research frontier over the past 10–15 years is represented by tertiary creep modelling and the estimation of service life. Tertiary creep, characterized by an accelerating strain rate, is exclusively attributed to internal damage—specifically the formation and coalescence of microcracks and voids under constant stress. Consequently, recent models, such as those developed by Cao et al. [39] and Wang et al. [40], utilize an internal damage variable to describe the evolution of this structural degradation.

These creep-damage models can simulate the entire creep cycle until failure, providing a far more reliable method for estimating the time to failure (t_r) than the simple extrapolation of secondary creep data. Furthermore, specialized literature indicates increased complexity in salt behaviour under multi-stage conditions, noting that the relationship between stress and creep rate may be non-monotonic at intermediate stress levels [32, 39]. This necessitates a critical analysis of the applicability of Norton's law and highlights the need for more sophisticated, comprehensive models that encompass the full spectrum of experimentally observed behaviour.

While the body of knowledge regarding salt rheology is vast, the precise characterization of local deposits, such as the one at Slănic Prahova, remains a fundamental engineering necessity. The results of this study aim to provide a quantifiable contribution by establishing the rheological parameters specific to the investigated massif. The primary objective of this research is to investigate and model the viscous-plastic behaviour of salt under multi-stage uniaxial loading.

 vol. 32, issue 1 / 2026
pp. 34-54

To achieve this goal, the following specific objectives were established: (a) first, the experimental determination of axial, lateral, and volumetric creep curves as a function of time; (b) second, a critical analysis of secondary creep through the calibration of Norton's law, aiming to establish the stress exponent and evaluate the model's accuracy in light of the potentially non-monotonic behaviour of the creep rate; (c) third, modelling the time-dependency of ultimate strain for long-term predictions; (d) finally, the quantification of tertiary creep and the estimation of service life (t_r) through exponential extrapolation—a vital step for operational safety assessment.

The structure of this paper is designed to methodically address these objectives. The following section details the experimental methodology and materials used. Subsequently, the paper presents the results of the secondary creep rate analysis and the modelling of Norton's law. A distinct segment is dedicated to the detailed analysis of tertiary creep and service life estimation. The paper concludes with final findings that synthesize the major contributions and indicate future research directions necessary for the development of advanced constitutive models.

2. Creep of rock salt: fundamentals and microscopic mechanisms

Creep is a phenomenon of slow and continuous deformation of a solid material under constant stress over a long period, even at stress levels below the yield strength [39, 40]. Unlike elastic deformation, which is reversible, or rapid plastic deformation, creep is a time-dependent plastic deformation [12, 13, 17, 38, 40]. This phenomenon is particularly important to study in rock salt, as salt exhibits significant viscous-plastic behaviour even at ambient temperatures. Understanding salt creep is essential in various engineering fields, specifically: (a) stability of room and pillars: salt mines are vast underground structures. Creep can lead to subsidence or pillar instability, affecting long-term safety and structural integrity; (b) radioactive waste disposal: salt formations are considered ideal locations for the final disposal of radioactive waste. The capacity of salt to "self-heal" through creep, sealing fractures and isolating waste from the environment, is a major advantage. However, it is essential to understand the rate and behaviour of creep to ensure repository integrity over thousands of years; (c) other geotechnical applications: Salt creep is also relevant in the design of storage caverns for natural gas or hydrocarbons, where maintaining volume and structural integrity is paramount [2, 3, 5, 9, 12].

What makes salt a unique material is its cubic crystal structure and relatively weak ionic bonds, which allow dislocations and other deformation mechanisms to activate at much lower stresses and temperatures compared to other rocks. Thus, salt does not behave merely as an elastic or plastic material, but also as an extremely viscous fluid, whose deformation continues over time under constant load.

To understand how salt deforms under constant stress over long periods, it is essential to analyse the processes or mechanisms occurring at the microscopic level within its crystalline structure. Salt creep is not the result of a single mechanism, but a complex combination of interdependent phenomena, dominant depending on the stress level, temperature, and material composition [41]. The primary mechanisms involved in salt creep are:

- Dislocation glide: This is among the most important creep mechanisms in salt at moderate temperatures and higher stresses. The movement of dislocations leads to the permanent deformation of the crystal. The dislocation glide rate is influenced by dislocation density, mobility, and the presence of obstacles (such as impurities or other dislocations).
- Diffusion creep (Nabarro-Herring and Coble creep): At high temperatures and low stresses, the diffusion of atoms through the crystal lattice (volume diffusion, called Nabarro-Herring creep) or along grain boundaries (grain-boundary diffusion, called Coble creep) becomes a predominant mechanism. Atoms migrate from areas of high compressive stress to areas of tensile stress, resulting in mass redistribution and, consequently, slow and continuous deformation. This mechanism is more efficient in fine-grained materials where the total grain-boundary surface area is high.
- Grain boundary sliding: This mechanism involves the relative motion of individual salt grains against each other. Although the grains remain internally undeformed, their sliding at interfaces contributes to the macroscopic deformation of the salt mass. This process is often assisted by diffusion or the presence of minor fluid phases at grain boundaries.
- Solution-precipitation creep: In the presence of water (either as fluid inclusions or interstitial moisture), salt can dissolve in high-stress areas and reprecipitate in low-stress areas. This dissolution-precipitation cycle facilitates mass transport and contributes significantly to creep, especially under hydrothermal conditions. This mechanism can be particularly relevant in salt deposits containing a certain amount of interstitial water or fluid inclusions.

Revista Minelor – Mining Revue
ISSN-L 1220-2053 / ISSN 2247-8590

Influence of temperature and stress: An increase in temperature accelerates all creep mechanisms, especially those based on diffusion and dislocation glide, as additional thermal energy provides the atoms and dislocations with the mobility necessary to overcome energy barriers. At low stresses, diffusion creep may be dominant. As stress increases, dislocation glide becomes increasingly important. There is a non-linear relationship between stress and creep rate, often described by power laws [42, 43, 44].

Influence of impurities [41]: The presence of impurities influences salt behaviour in several ways: (a) inclusions of clay, anhydrite ($CaSO_4$), or other insoluble minerals can have a significant impact on creep behaviour. These can act as obstacles to dislocation movement, strengthening the salt and reducing the creep rate. Conversely, if impurities form continuous layers or interconnected networks, they may facilitate grain boundary sliding or create preferential pathways for diffusion; (b) the presence of water or brine can significantly reduce creep resistance, particularly through the solution-precipitation mechanism.

Understanding these mechanisms is fundamental for interpreting experimentally obtained creep curves and for modelling salt behaviour in long-term engineering applications.

3. Experimental research and methodology

This section details the methodology employed to investigate the mechanical and rheological properties of the Slănic Prahova rock salt, providing a robust foundation for the interpretation and validation of the obtained results. Laboratory research represents the most direct method for investigating the creep properties of rocks, offering the advantages of long-term observation, cost-effectiveness, and strict control over experimental conditions. This approach enables the determination of relevant parameters essential for establishing constitutive creep models.

The research strategy followed in this study is synthesized in the methodological workflow presented in Figure 1. The process initiates with the preparation of cylindrical specimens from Slănic Prahova deposit, followed by preliminary uniaxial compressive strength (UCS) testing to define the appropriate stress levels for the creep phase. As illustrated in the workflow, the core of the investigation consists of a multi-stage creep test (Stages I to VI), providing the empirical data required for constitutive modelling. This structured approach allows for the simultaneous calculation of secondary creep rates and the identification of complex rheological coefficients (α, β, γ, χ, C_F). Ultimately, the workflow demonstrates how the onset of tertiary creep (Stage VI) and the resulting failure mechanisms are utilized through exponential extrapolation to achieve reliable long-term stability predictions.

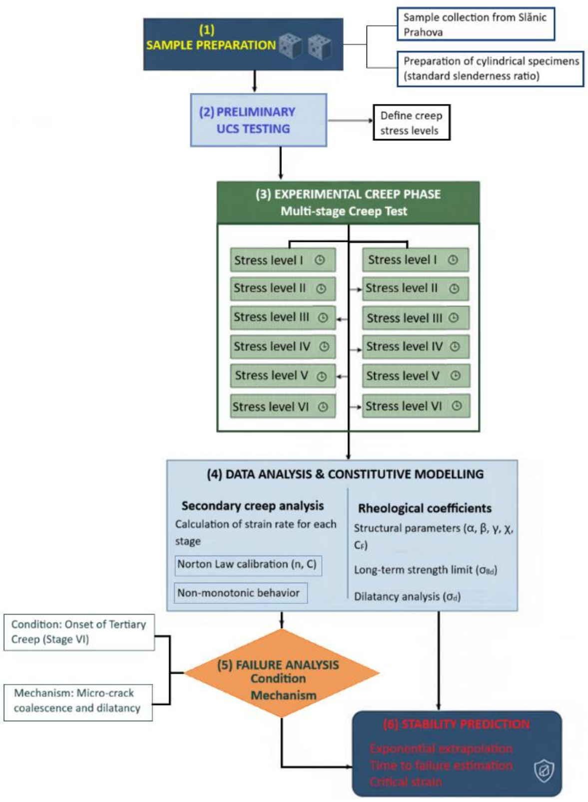

Fig.1. Methodological workflow for the rheological characterization of Slănic Prahova rock salt, illustrating the transition from experimental multi-stage loading to constitutive modelling and long-term stability prediction

3.1. Materials and equipment

Materials

The rock salt specimens used in these studies were sampled from Slănic Prahova deposits. Rock salt is a typical crystalline rock, and its rheological behaviour is a macroscopic reflection of internal microstructural changes occurring under external conditions, such as stress and temperature. Mineralogical composition plays a significant role; generally, pure salt exhibits superior rheological properties—specifically, a higher deformation capacity—compared to salt containing impurities or interlayers, where their presence may limit the overall deformation of the material. The variations in uniaxial compressive strength ($\bar{R}_c$, MPa) across different boreholes, as shown in Table 1, confirm the inherent heterogeneity of the deposit [41].

Table 1. Studied salt varieties

No	Salt variety	Borehole	$\bar{R}_c$ (MPa)
1	Rock salt with impurities, white-grey, saccharoidal	P1	19.96
2	Rock salt with impurities, grey-white, saccharoidal	P3	22.76
3	Rock salt with impurities, white-grey, saccharoidal	P4	25.05
4	Rock salt with impurities, grey, saccharoidal	B3	14.7

Test equipment

To determine the rheological and dilatancy characteristics of the salt, specialized testing equipment was utilized, capable of applying and maintaining constant loads over extended periods while simultaneously recording deformations. The creep tests were conducted under uniaxial compression conditions, meaning the load was applied along a single axis without active lateral confining pressure, allowing for the unconstrained observation of lateral strains.

The loading system involved the application of stress increments (constant stress levels) over prolonged durations. Strain measurements included: longitudinal strain ($\boldsymbol{\varepsilon}_l$), transverse strain ($\boldsymbol{\varepsilon}_t$), and volumetric strain ($\boldsymbol{\varepsilon}_v$). he monitoring systems enabled the continuous recording of these strains as a function of both time and applied load [41]. Given that temperature is a major factor influencing the creep properties of salt, the tests were performed under controlled temperature conditions (ambient temperature).

3.2 Specimen preparation and creep testing methodology

The samples were prepared as cylindrical specimens with standardized geometry (maintaining an appropriate slenderness ratio) to minimize end-friction effects and ensure a homogeneous state of stress [41]. The compressive strength of the specimens was determined prior to the creep tests, providing the necessary context for the applied stress levels.

The creep tests were conducted across various stress increments. The procedure consisted of the successive application of six distinct stress levels, maintaining each constant load for a specific duration while recording the accumulated strains. The applied loading levels were established based on the uniaxial compressive strength value. The duration of each stress step was variable, ranging from approximately 7 days for the first increment to over 100 days in total, culminating in failure during the final stage.

The total strain accumulated by the specimen is the sum of the strains from all previous steps plus the specific deformation of each current increment. The tests were continued until material failure occurred, manifested by a sudden acceleration in the strain rate (tertiary creep), thus fulfilling the failure criterion. The duration of each step was sufficient to allow for the attainment and identification of the secondary (steady-state) creep stage.

3.3 Data processing and analysis criteria

The recorded raw strain and time data were processed to generate the graphs and values used in the analysis. Stress-strain curves (longitudinal, transverse, and volumetric) were generated—essential for identifying the behavioural zones of the rock salt—along with strain-time curves for each increment, illustrating the evolution of creep.

Assessment of creep rate and rheological dilatancy threshold

Strain rate in the secondary creep domain: the axial strain rate ($\dot{\varepsilon}_s$) was calculated by differentiating the strain-time curves. The identification of the steady-state creep rate ($\dot{\varepsilon}_s$) was achieved by determining the minimum or constant slope of the strain-time curve during the stationary creep phase. These values were subsequently correlated with the applied stress to establish the σ vs. ($\dot{\varepsilon}_s$) relationship required for Norton modelling.

 vol. 32, issue 1 / 2026
pp. 34-54

Dilatancy threshold (**σ_d**): To analyse the compressibility-dilatancy behaviour, dilatancy curves (volumetric strain as a function of stress) were plotted. The dilatancy threshold—defined as the point where volumetric strain ceases to be compressive and becomes dilatant—is a critical indicator: a lower dilatancy threshold indicates reduced internal stability of the rock [41].

Deformation behaviour model

Based on the stress-strain curves [41], the behaviour was divided into five distinct zones, which serve as the basis for interpreting the results:

- Viscous-elastic deformation: The initial phase marked by non-linearity and a rapid decrease in volume due to the closure of pores and micro-fissures.
- Elastic behaviour: In this zone, cracks continue to close, leading to increased linearity and homogeneity up to a fracturing limit (typically 0.5–0.7 of the ultimate strength).
- Controlled crack propagation: This represents the onset of dilatancy, marked by a deviation from linearity, indicating a transition toward ductile behaviour.
- Continuous crack growth: The development and coalescence of cracks, accompanied by an increase in porosity and permeability, with a significant deviation from linearity. This phase marks unstable cracking and intensified dilatation, serving as a precursor to tertiary creep.
- Post-failure: The phase where stress decreases, but deformations (longitudinal, transverse, and volumetric) may continue to increase, reflecting post-critical behaviour until the ultimate residual strength is reached.

These data processing methods and analysis criteria enabled a detailed investigation of the mechanical and rheological behaviour of Slănic Prahova salt, confirming the presence of all three creep stages and a complex behavioural spectrum.

3.4 Theoretical constitutive models

The processing of experimental data was based on two fundamental constitutive models to describe the viscous-plastic behaviour of the salt.

Secondary creep modelling (Norton's law)

Behaviour during the secondary (steady-state) creep stage is most frequently described by Norton's power law, which establishes a relationship between the steady-state creep rate ($\dot{\varepsilon}_s$) and the applied stress (σ):

To model the relationship between the secondary creep rate and stress, Norton's power law was applied, a common constitutive form for creep:

$$\dot{\varepsilon}_s = A\sigma^n exp\left(-\frac{Q}{RT}\right) \tag{1}$$

Since the tests were performed at a constant temperature (not explicitly stated, but implicit), the equation can be simplified to:

$$\dot{\varepsilon}_s = C\sigma^n \tag{2}$$

Where C is a constant that incorporates the effects of temperature:

$$C = Aexp\left(-\frac{Q}{RT}\right) \tag{3}$$

and n is the stress exponent (or creep exponent), whose value is used to deduce the dominant deformation mechanism (diffusion, dislocation climb, etc.).

To calibrate the parameters C and n, the equation is linearized through natural logarithms, allowing for the application of linear regression on the transformed data:

$$ln(\dot{\varepsilon}_s) = ln(C) + nln(\sigma) \tag{4}$$

This form allows for the application of linear regression on $ln(\dot{\varepsilon}_s)$ as a function of *ln(σ)*.

Tertiary creep modelling and estimation of time to failure

Tertiary creep is characterized by an acceleration of deformation caused by internal damage. Although complex creep-damage models are ideal, an initial estimation of the time to failure (t_r) can be achieved through the exponential extrapolation of data from the tertiary stage, considering the function:

$$\varepsilon(t) = k \times e^{mt} \tag{5}$$

 vol. 32, issue 1 / 2026
pp. 34-54

By linearizing this relationship, the time to failure (tr) can be determined, assuming a critical failure strain (ε_{critic}):

$$ln(\varepsilon_{critic}) = m \times t_r + ln(k) \tag{6}$$

4. Results and discussion on secondary creep and constitutive modelling

This section presents the results of the quantitative analysis of the secondary creep stage and performs the calibration of the Norton law constitutive model, basing the discussion exclusively on the experimental data and the obtained graphical representations.

4.1. Analysis of general viscous-plastic behaviour and creep curves

The rheological investigation confirmed the typical viscous-plastic behaviour of the salt. The analysis of the rheological curves is fundamental for understanding the behavioural transitions. (Figure 2).

These graphical representations allow for the segmentation of the deformation behaviour into the five zones described in Section 3, and the identification of the rheological dilatancy threshold ($\boldsymbol{\sigma}_d$).

Based on the analysis of the creep curves and the processing of experimental data, the values for the rheological coefficients (γ, α, β, χ), the creep coefficient (C_F), the strain at the elastic limit, the long-term strength limit (σ_{lld}), and the stability domain were determined, as shown in Table 2 [41]. These parameters quantify the viscous-plastic behaviour of the salt and are fundamental for formulating constitutive models and predicting the long-term behaviour of the salt massif in engineering applications. The results also indicate a stability period ranging from 7 to 11 years, potentially reaching up to 15 years, after which the salt enters a domain of medium instability [41].

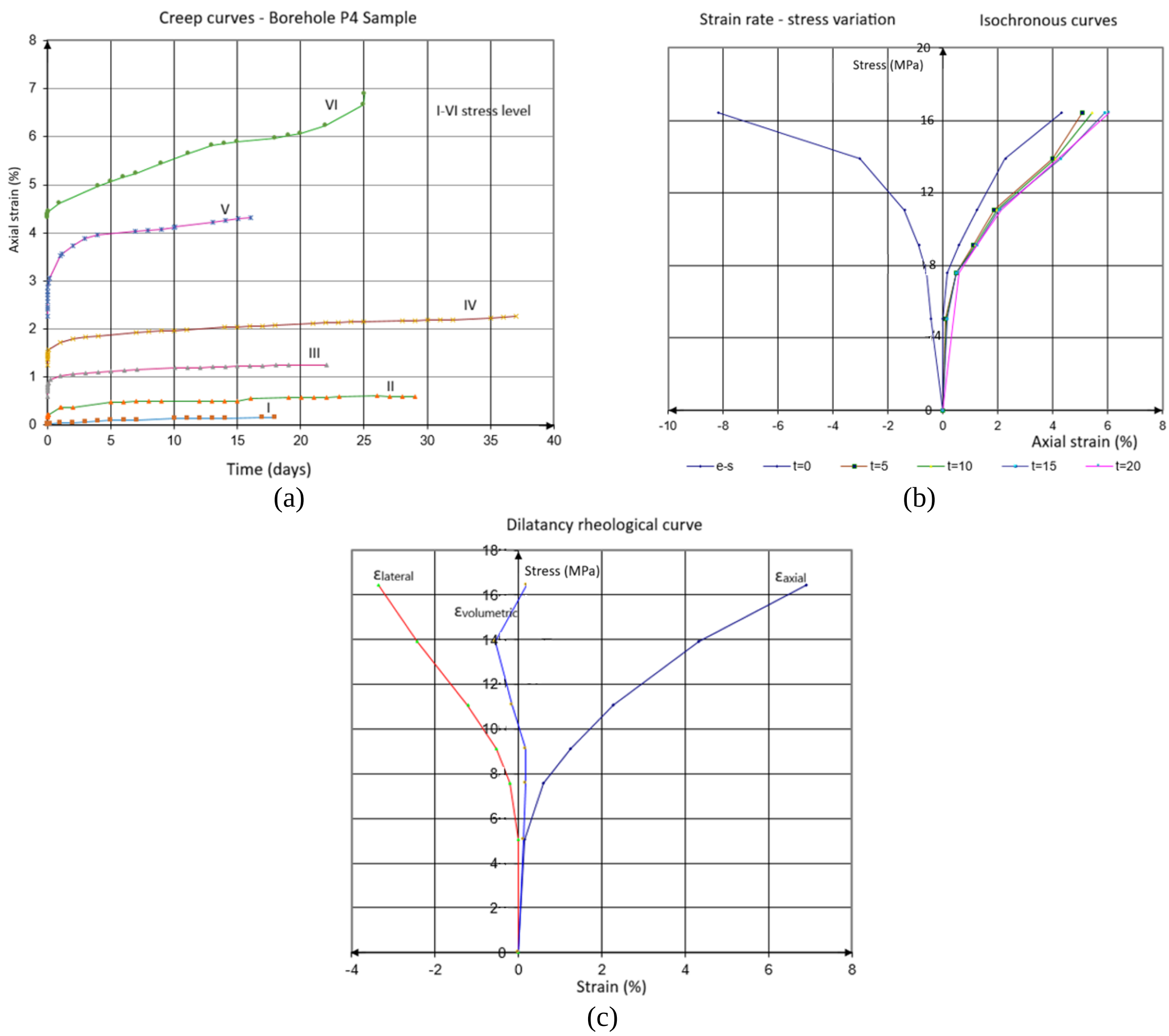

(a) (b) (c)

Fig.2. Rheological characteristic curves – Borehole P4 Sample

Revista Minelor – Mining Revue
ISSN-L 1220-2053 / ISSN 2247-8590 vol. 32, issue 1 / 2026
pp. 34-54

Table 2. Centralized values of rheological coefficients

Borehole specimen	Rheological coefficients				Creep coefficient, C_F	Strain at elastic limit (%)	Long-term strength limit, σ_{lld} (MPa)	Stability field
	γ	α	β	χ				
P1	0.695651	0.57	0.26834	0.16588	0.61816	0,016524	12.35617	0.2-0.3
P3	0.719779	0.45	0.53847	0.32931	0.611574	0.017246	14.18615	
P4	0.692259	0.64	0.37307	0.22714	0.608833	0,019172	15.66898	
B3	0.701271	0.53	0.3879	0.25254	0.651044	0,014619	8.683657	

The rheological parameters identified in Table 2 (γ, α, β, χ, C_F) provide a quantitative framework for the hereditary behaviour of Slănic Prahova salt. According to the hereditary theory of Volterra and Rabotnov, the strain observed at any given time is a function of the material's entire loading history. To facilitate engineering calculations, this study utilizes generalized rheological functions—specifically the Abel and Rozovski kernels.

Within this framework, α serves as the Abel kernel exponent, characterizing the rate of structural stabilization, while γ, β, and χ define the non-linear memory functions of the salt. Furthermore, the creep coefficient (C_F) is essential for both the rheological classification of the salt and the evaluation of its long-term strength limit (σ_{lld}). These coefficients are not merely descriptive; they allow for the determination of time-dependent geomechanical properties, such as E(t), μ(t), and G(t), which are essential for predicting the long-term stability and structural integrity of the salt massif in mining applications.

4.2. Strain rate in the secondary creep stage and non-monotonic behaviour

The secondary creep rate ($\dot{\varepsilon}_s$) was calculated for each increment (Table 3) as the minimum (quasi-constant) slope of the axial strain-time curves:

$$\dot{\varepsilon}_s = \frac{\varepsilon_2 - \varepsilon_1}{t_2 - t_1} \tag{7}$$

where ε_1 where is the strain at time t_1, and ε_2 is the strain at time t_2 (two representative points (ε_1, t_1) and (ε_2, t_2) within the secondary stage).

The values in Table 3 are used for modelling Norton's law, which establishes a linear relationship in logarithmic space.

Table 3. Strain rate values in the secondary creep stage

Stress level	Stress, σ (MPa)	$\dot{\varepsilon}_s$ (%/day)	ln(σ)	$ln(\dot{\varepsilon}_s)$
I	3.675	0.00588	1.301	-5.137
II	4.41	0.01475	1.484	-4.219
III	7.35	0.02055	1.995	-3.885
IV	8.82	0.01629	2.177	-4.117
V	10.29	0.01217	2.331	-4.409
VI	11.76	0.04754*	2.465	-3.047
* this value is less representative of a "true" secondary stage due to the rapid onset of tertiary creep.				

The graphical representation of the results obtained visually illustrates the discrepancy from the ideal behaviour (Figure 3).

The variation of the steady-state creep rate as a function of stress (Figure 3) reveals the complex kinetic response of Slănic Prahova salt. The curve is characterized by a clear non-monotonic interval between 7.35 and 10.29 MPa, where structural hardening leads to a 40% reduction in velocity. This physical behaviour necessitates the use of advanced hereditary kernels, such as Rozovski model, to account for the material's memory and internal structural shifts. The graphical representation of the results visually illustrates a clear discrepancy from idealized monotonic behaviour. The evolution of the steady-state creep rate (ϵ˙s) as a function of applied stress (σ) reveals three distinct kinetic zones:

1. Initial linear-viscous zone (3.67 – 7.35 MPa): In this interval, the creep rate increases from 0.00588 %/day to 0.02055 %/day. Quantitatively, a doubling of the stress results in an approximately 3.5-fold increase in the deformation rate. This stage is described using the Abel kernel, where the exponent α characterizes the initial stabilization of the material's fractional-exponential memory.

 vol. 32, issue 1 / 2026
pp. 34-54

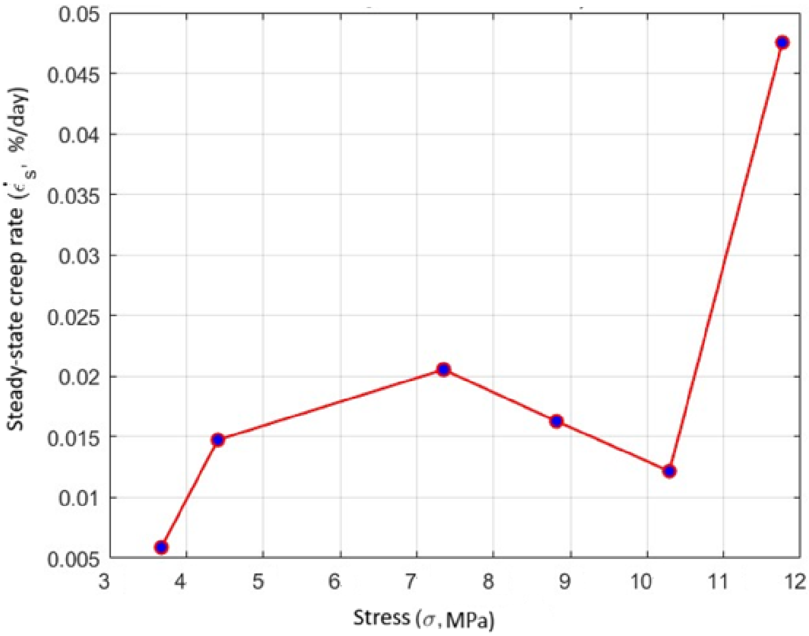

Fig.3. Variation of secondary creep rate as a function of applied stress for the tested salt

2. Non-monotonic hardening zone (7.35 – 10.29 MPa): A significant physical anomaly is observed as the stress increases; the creep rate decreases by approximately 40%, falling to 0.01217 %/day. This reduction in velocity despite an increasing load provides quantitative evidence of structural hardening. To capture this complex behaviour, Rozovski kernel parameters (β, γ, χ) are essential, as they account for the non-linear "memory" and interaction effects under intermediate stress levels.

3. Critical transition to tertiary creep (10.29 – 11.76 MPa): At the final stress level of 11.76 MPa, the creep rate exhibits a sharp exponential surge to 0.04754 %/day. This represents a 3.9-fold acceleration compared to the previous stage, signalling that the stress has approached the long-term strength limit (σlld).

The observed non-monotonic behaviour, highlighted by the inflection point in Figure 3, suggests that the secondary creep rate does not always increase with applied stress due to internal structural adjustments. This unexpected decrease can be attributed to several factors:

a) Strain hardening effects induced by cumulative loading;
b) A complex shift in the deformation mechanism at intermediate stress levels;
c) Specific microstructural effects of Slănic Prahova salt that influence defect mobility.

Using the identified creep coefficient ($C_F = \chi/\beta$), this transition point allows for the quantitative estimation of the safety threshold for underground excavations. This confirms that the identified rheological parameters are not mere numerical outputs but fundamental indicators of the rock's long-term stability.

4.3. Calibration and limitations of the Norton model

The calibration of the model $\dot{\varepsilon}_s = C\sigma^n$ was performed through linear regression on the logarithmically transformed data (Figure 4). By performing the linear regression, the slope of the line (n) was found to be approximately 1.57 and the intercept (ln(C)) ≈ -10.74, while the coefficient of determination was $R^2 \approx 0.58$. Thus, the power law that approximately describes the experimental data is:

$$\dot{\varepsilon}_s \approx exp(-10{,}74)\sigma^{1{,}57} \approx 2{,}16 \times 10^{-5}\sigma^{1{,}57} \tag{8}$$

To determine the constitutive parameters, the previous data was analysed in a log-log coordinate system (Figure 4). While Figure 3 highlighted the physical anomalies, Figure 4 provides the quantitative calibration of the Norton power law, yielding a stress exponent n≈1.57. The moderate $R^2 \approx 0.58$ is a direct statistical reflection of the physical deviations (the hardening and the tertiary surge) discussed in the previous section. Thus, the mathematical dispersion confirms the phenomenological complexity rather than experimental error. The quantitative breakdown of the regression analysis reveals several key phenomenological aspects:

Statistical correlation (R^2): The coefficient of determination ($R^2 \approx 0.58$) indicates a moderate correlation. However, this does not signify experimental imprecision but rather captures the inherent phenomenological complexity of Slănic Prahova rock salt. This statistical value is directly influenced by the non-monotonic fluctuations observed at ln(σ) values between 4.2 and 4.6 (stages IV and V), where the material's response deviates from the idealized power-law prediction.

vol. 32, issue 1 / 2026
pp. 34-54

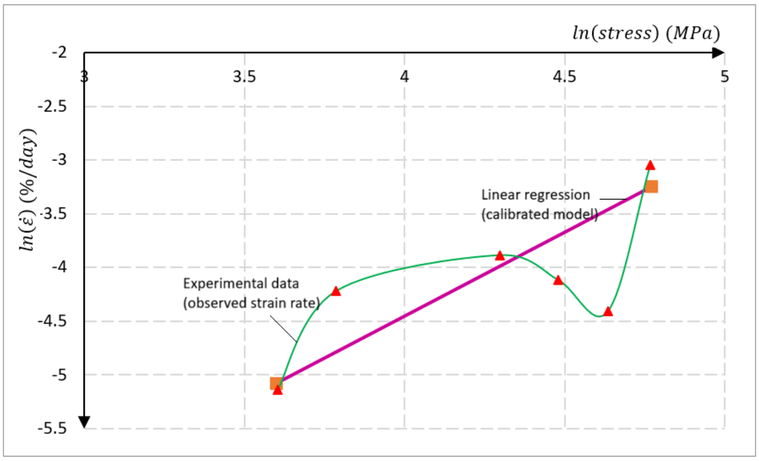

Fig.4. Model calibration via linear regression on logarithmically transformed data

Maximum negative deviation: This is most prominent during stage V (ln(σ)≈2.33), where the experimental value of -4.409 sits significantly below the regression line. Quantitatively, this represents the point of maximum structural hardening, confirming the non-monotonic behaviour where the deformation rate decreases contrary to simplified theoretical expectations.

Transition to failure: At ln(σ)≈2.46 (Stage VI), the experimental point surges to -3.047, crossing the regression line upwards. This surge represents a 3.9-fold increase in the actual strain rate compared to the previous stage, confirming the rapid onset of tertiary creep and the accumulation of internal damage.

Conclusion on model validity: While the experimental points do not align perfectly with the linear trend, the regression provides a robust average representation of the salt's viscous behaviour. The quantitative mismatch in stages IV and V is not an error but a physical justification for using more advanced hereditary kernels, such as Rozovski kernel. These models utilize the coefficients β and γ specifically to account for the non-linearity and the material's "memory" of its previous deformation history.

4.4. Discussion of parameters and model limitations

The value of the parameter n ≈ 1.57 suggests a predominance of diffusion-controlled creep mechanisms (such as Coble or Nabarro-Herring), indicating that mass transport at grain boundaries is the limiting factor of the deformation rate. Consequently, creep mechanisms based on diffusion or grain boundary sliding could be dominant in the tested salt, although the exact value requires a more in-depth analysis of the mechanisms. It should be noted that this relationship is an approximation based on a limited number of points and the hypothesis of a constant temperature. The previously observed non-monotonic behaviour, as well as the relatively low value of R^2 (≈0.58), limits the precision of this simplified model across the entire stress interval.

The relatively low R^2 value confirms that a single power-law formulation (Norton's Law) serves only as a first-order approximation for this specific deposit. Throughout the six loading increments, the salt undergoes distinct kinematic regimes. At lower stress levels, the exponent n≈1.57 aligns with the dominance of diffusion-based mechanisms. However, the experimental deviation from logarithmic linearity (as illustrated in Figure 4) suggests a transition toward mechanisms controlled by dislocation glide and, subsequently, the initiation of micro-cracking (damage) during the later stages. This transition explains the fluctuations in the creep rate that preclude a strictly monotonic increase, thereby limiting the explanatory power of the linearized Norton model over the entire stress spectrum.

Although Norton's Law predicts linearity in a logarithmic representation, the plot exhibits non-linear behaviour due to the following factors: (1) the scope of Norton's law: Norton's power-law formulation best describes steady-state (secondary) creep at constant temperatures and stress levels where a single creep mechanism predominates. The behaviour of rock salt can be more complex, involving multiple creep mechanisms (such as, dislocation glide, diffusion) that may become dominant at different stress levels or temperatures. When several mechanisms contribute simultaneously, the logarithmic relationship may deviate from linearity; (2) influence of tertiary creep: in particular, the final data point (at 117.6 daN/cm²) shows a sharp increase in the creep rate ($ln(\dot{\varepsilon}_s)$ jumping from -4.409 to -3.047). This acceleration indicates the onset of the tertiary creep stage, which is not accounted for by Norton's law (as the latter pertains strictly to secondary creep). During tertiary creep, damage phenomena—such as void formation and micro-cracking—

occur, leading to rapid strain acceleration and deviation from linear logarithmic behaviour; (3) variations in the creep mechanism: the decrease in creep rate is an issue that warrants more detailed study, as it may suggest a shift in the deformation mechanism. It is possible that, at intermediate stress levels, a mechanism less sensitive to stress increases becomes active, or even a temporary 'strain hardening' mechanism under specific stress conditions; (4) experimental data and dispersion: there is always an inherent degree of scatter in experimental data. While a general trend can be observed, individual data points may deviate from a perfectly linear fit.

This implies that: (a) Norton's Law as a first-order approximation: although it does not provide a perfect fit across the entire range, the application of Norton's Law (with a slope of $n \approx 1.57$ and an intercept of $\ln(C) \approx -10.74$) remains a standard approach for modelling creep behaviour, yet it demonstrates the limited precision of Norton model. It is crucial to note that this law is an approximation and fails to perfectly describe the behaviour of rock salt across the full stress spectrum, particularly due to the onset of tertiary creep at high stress levels and non-monotonic behaviour at intermediate stresses; (b) the necessity for more complex models: the observed non-linearity suggests that for a more accurate description of rock salt creep over a wide range of stresses, more sophisticated constitutive models may be required (for example, those incorporating transitions between creep mechanisms or separately modelling primary, secondary, and tertiary creep).

This lack of statistical correlation stems from the non-monotonic behaviour and the inherent inhomogeneity of the rock salt from Slănic Prahova. For reliable engineering predictions, it is imperative to employ more advanced viscous-plastic models capable of integrating either strain-hardening effects at intermediate stresses or incipient damage.

4.5. Modelling of total accumulated axial strain

The total accumulated axial strain of the specimen at the end of each loading stage (ε_f) was analysed as a function of the cumulative final time (t_f), providing insight into the long-term behaviour of the material. Since the total duration of the tests varied for each loading step, the analysis focused on the axial strain reached at the conclusion of each stage (or at the last available data point), as shown in Figure 5.

A consistent increase in the axial strain reached at the end of the test is observed for each stage as the applied stress increases. This represents an expected trend, as higher stress levels inevitably lead to more significant deformation over time. The relationship between stress and final strain does not appear to be perfectly linear, exhibiting a degree of non-linearity. The increase in strain becomes more pronounced at higher stress levels, particularly during stages V and VI.

To model the relationship between the final time (t_f) and the total accumulated axial strain (ε_f), two types of functions were proposed and evaluated: a power-law model (Model 1) and a simple exponential model (Model 2).

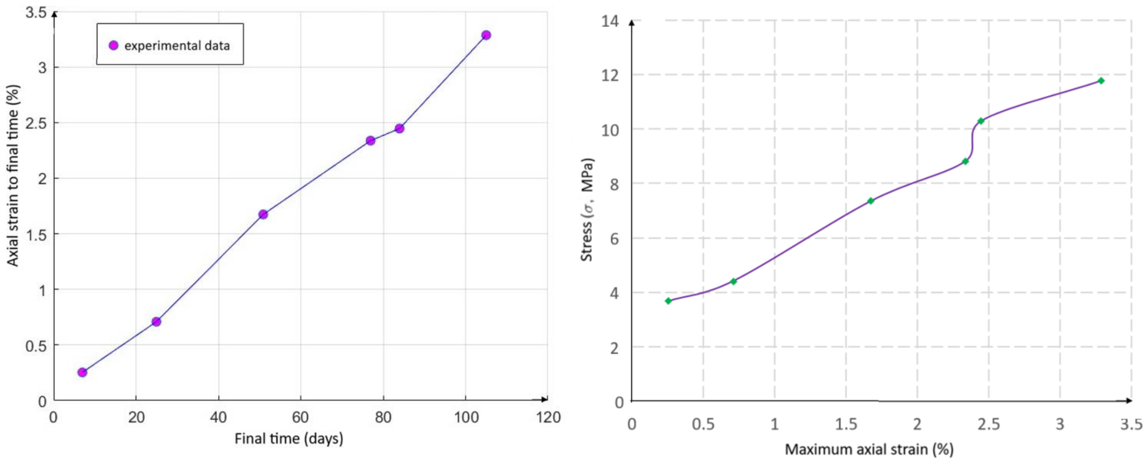

(a) (b)

Fig.5. Total accumulated axial strain as a function of the final time of each loading stage (a) and as a function of the applied stress (b)

The power-law function for Model 1 is defined as:

$$\varepsilon_f = a \cdot t_f^b \quad (9)$$

vol. 32, issue 1 / 2026
pp. 34-54

By taking the logarithm of equation (9) and applying linear regression to the experimental data, the power-law model takes the following form:

$$\varepsilon_f \approx 0.055 \cdot t_f^{0.78} \tag{10}$$

The simple exponential function for Model 2 is defined as:

$$\varepsilon_f = c \cdot e^{d \cdot t_f} \tag{11}$$

By taking the logarithm of equation (11) and applying linear regression to the experimental data, the simple exponential model is expressed as:

$$\varepsilon_f \approx 0.171 \cdot e^{0.016 \cdot t_f} \tag{12}$$

To evaluate which model best fits the experimental data, the coefficient of determination (R^2) was calculated for both regressions. An R^2 value closer to 1 indicates a better fit (Table 4).

Table 4. Calculation of the R^2 coefficient for the considered models

Metric	Power-law model	Simple exponential model
Average $\overline{ln(\varepsilon_f)}$	0.289	0.289
Total Sum of Squares (SST)	4.693	4.693
Sum of Squared Residuals (SSR)	0.618	8.689
R^2	0.868	-0.851

An R^2 value of approximately 0.868 for the power-law model indicates a reasonably good fit with the experimental data. Roughly 86.8 % of the variability in ln(ε_f) is explained by the linear model in ln(t_f). Conversely, the negative R^2 for the simple exponential model suggests a very poor and inadequate fit. This model fails to accurately describe the observed relationship.

Consequently, the power-law model expressed by equation (2) provides a significantly better fit for the experimental data regarding final strain as a function of final time compared to the simple exponential model (Figure 6). The red line (power-law model) clearly follows the trend of the experimental data points more closely than the green line (simple exponential model), confirming the quantitative analysis based on R^2.

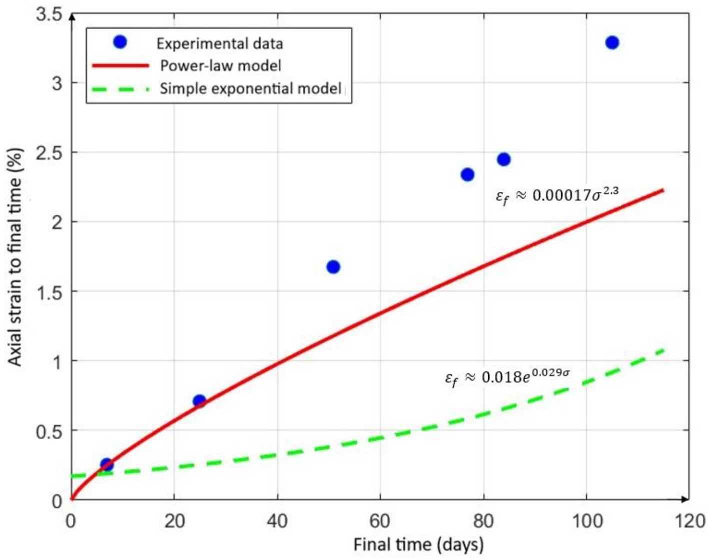

Fig.6. A comparison of experimental data with power-law and simple exponential models for time-dependent ultimate strain

The statistical superiority of the power-law model over the simple exponential model is quantitatively validated by the alignment of experimental data points in Figure 6. The analysis reveals the following numerical insights:

Model accuracy (R^2): Roughly 86.8 % of the variability in the ultimate axial strain (ε_f) is accurately explained by the power-law model ($\varepsilon_f \approx 0.00017\sigma^{2.3}$). In contrast, the exponential model ($\varepsilon_f \approx 0.018e^{0.029\sigma}$) yields a negative R^2, indicating that it fails to capture the fundamental curvature of the failure trend.

Deviation at Long-Term Intervals (t > 80 days): The quantitative gap between the two models widens significantly as the time to failure increases. At approximately 105 days, the experimental axial strain reaches its maximum value of ~3.3 %. While the power-law model (red line) predicts a value of approximately 2.2 % (underestimating by 33 %), the exponential model (green line) predicts only ~1 %, resulting in a massive 70 % underestimation of the actual deformation.

Predictive reliability: The power-law model follows the upward trajectory of the experimental points, particularly as they accelerate toward failure after day 80. This confirms that the rock salt failure mechanism is non-linear and time-dependent, making the simple exponential approach mathematically inadequate for long-term stability estimations in Slănic Prahova mine.

4.6. Modelling the relationship between final strain and stress

To understand the dependency of final strain on applied stress, several mathematical models were tested using the final axial strain reached at each loading stage, as shown in Table 5.

Table 5. Evaluation of mathematical models

Considered mode	**Mathematical expression**	**Result obtained through regression**	**R^2 value**
Linear model	$\varepsilon_f = m\sigma + c$	$\varepsilon_f \approx 0.026\sigma - 0.68$	≈0.88
Polynomial model	$\varepsilon_f = a\sigma^2 + b\sigma + c$	$\varepsilon_f \approx 0.0002\sigma^2 + 0.007\sigma - 0.13$	≈0.98
Exponential model	$\varepsilon_f = ae^{b\sigma}$	$\varepsilon_f \approx 0.018e^{0.029\sigma}$	≈0.95
Power-Law mode	$\varepsilon_f = a\sigma^b$	$\varepsilon_f \approx 0.00017\sigma^{2.3}$	≈0.97

Based on the R^2 coefficients, the following observations can be made: the linear model provides a reasonable fit; however, the polynomial (2nd degree), exponential, and power-law models exhibit significantly better correlations with the data, suggesting a non-linear relationship between stress and final strain. In this case, the second-degree polynomial model appears to offer the best preliminary fit, yielding the highest R^2 value.

The total strain evolution model, with a coefficient of determination of 0.98, demonstrates a strong non-linear correlation and is employed to predict the general long-term deformation trend of the rock mass. This provides an additional perspective compared to the Norton model, which is strictly based on the secondary creep rate.

4.7. Analysis of strains and strain rates

Deformation analysis and interpretation

To provide a more profound understanding of the analysed rock salt behaviour, a plot was generated to illustrate the evolution of strains. This provides a complex and informative visualization that combines the three-dimensional evolution of deformations with their two-dimensional projections as a function of time, as shown in Figure 7.

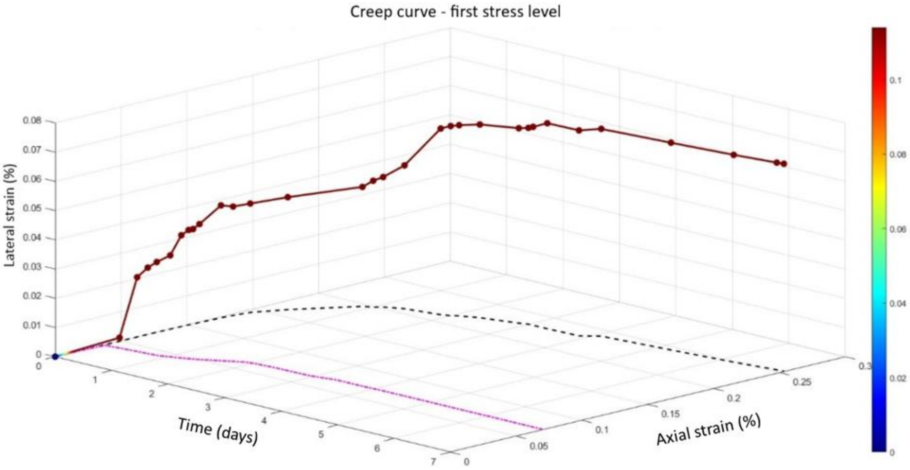

Fig.7. Three-dimensional evolution of axial, lateral and volumetric strain over time (illustrative graphical representation for the first loading stage)

vol. 32, issue 1 / 2026
pp. 34-54

The plot in Figure 8 provides a complex and informative visualization that combines the three-dimensional evolution of strains with their respective two-dimensional projections as a function of time. This representation allows for: (a) the visualization of the simultaneous evolution of axial and lateral strains over time; (b) the analysis of the projected curves on the time-axial strain plane (black dotted line) and the time-lateral strain plane (magenta dash-dot line) to observe the individual temporal variation of each strain component; (c) the correlation of the 3D curve colour (representing volumetric strain) with the evolution of the other two strain components and time.

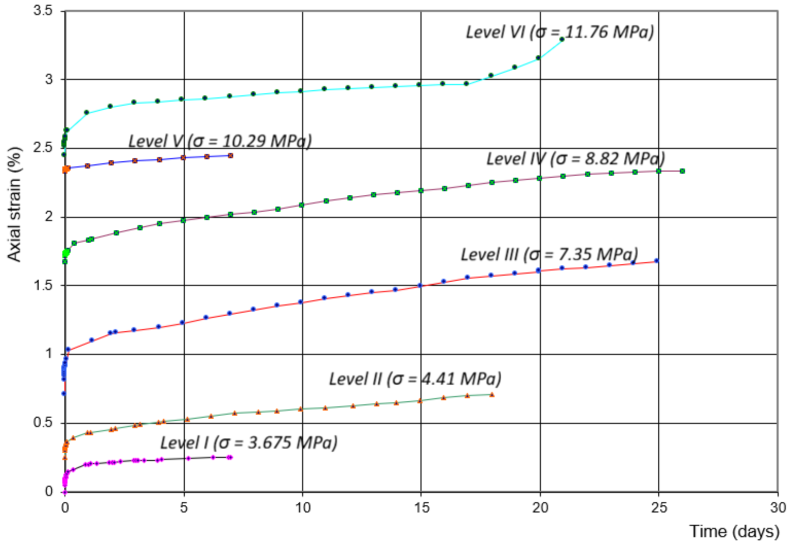

(a)

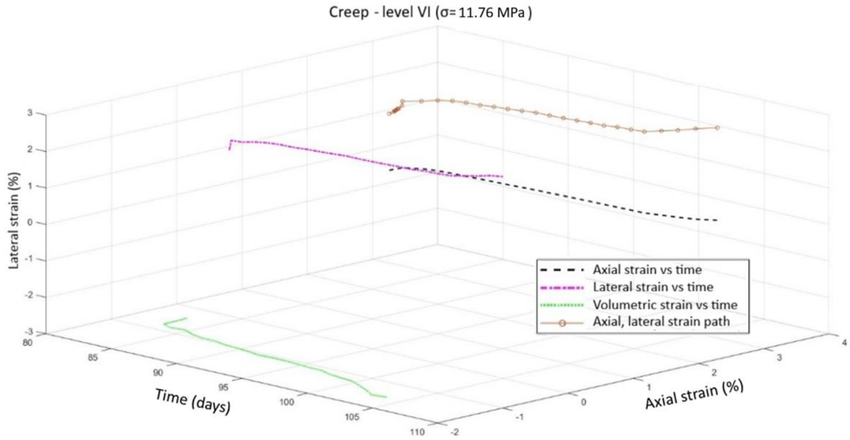

(b)

Fig.8. Creep curves (axial strain) for different stress level (a) and individual axial, lateral, and volumetric strain curves over time, alongside the 3D trajectory for the final loading stage (b)

General observations on the 3D creep plot: The curve originates at (0, 0, 0) at the initial time, indicating that all strain components are zero at the start of the test. During the initial moments, a rapid increase in both axial strain (characterized by a sharp upward trend of the curve) and lateral strain (indicated by displacement along the Z-axis) is observed. This phase corresponds to the initial loading stage and primary creep, where the strain rate is high and undergoes rapid deceleration.

At intermediate time intervals (the more "linear" portion of the curve), as time progresses, the rate of strain accumulation appears to diminish. The slope of the curve becomes less steep along both strain axes, which may correspond to the secondary or steady-state creep stage, where the strain rate remains relatively constant. A continued increase in axial strain is observed, alongside a potential deceleration or stabilization of the lateral strain.

Toward the end of the curve, at the final time, a shift in the strain rate may be observed. The curve might begin to exhibit a more pronounced curvature, indicating an acceleration of strains known as tertiary creep. Both axial and lateral strains continue to increase, potentially at higher rates than during the secondary stage.

vol. 32, issue 1 / 2026
pp. 34-54

Correlation with volumetric strain: The colour of the trajectory (within the 3D plot) represents the volumetric strain value at each point in time. As the curve is traced over time, the change in line colour indicates the evolution of volumetric strain. If the colour shifts toward the "warm" end of the spectrum (for example, from blue to red, where red indicates higher values), it signifies an increase in volumetric strain, indicating specimen dilatancy. A relatively constant colour along a segment of the curve would suggest a stable volumetric strain during that specific creep stage. It is expected that during the tertiary stage, concurrent with strain acceleration, a more rapid colour shift toward the "warm" spectrum will occur, suggesting a rapid volume change (dilation) prior to eventual failure. By examining both the curve geometry and colour evolution, a qualitative understanding is gained regarding the simultaneous evolution of axial and lateral strains over time and how this evolution correlates with the volumetric changes of the salt specimen undergoing creep.

Analysis of strains and strain rates for the final loading stage

For the final loading stage (stage VI), a pronounced acceleration of strain was observed, marking the onset of the tertiary creep stage, as shown in Figure 8. The individual analysis of the evolution of each strain component over time, coupled with the 3D trajectory, provides a comprehensive perspective on the material's behaviour.

Specific observations derived from Figure 8 include:

- temporal evolution of each strain component: the separate curves (black dotted line for axial strain, magenta dash-dot line for lateral strain, and green dotted line for volumetric strain) allow for the individual monitoring of how each strain component evolves over time. An accelerated increase is observed across all three components.
- 3D trajectory: the continuous line illustrates the combined evolution of axial and lateral strains over time. This trajectory becomes progressively steeper, reflecting the acceleration of creep phenomena.
- potential correlations: correlations can be established between shifts in the 3D trajectory and the individual evolution of each strain. For instance, an acceleration in axial strain growth can be associated with a rapid increase in volumetric strain and a distinct change in lateral strain.

To quantify this acceleration, the axial strain rate was calculated as a function of time for the final loading stage.

The axial strain rate at a given time point was approximated as the time derivative of the axial strain, calculated as the difference between axial strain values at two consecutive time points divided by the time interval between them:

$$\dot{\varepsilon}_{axial}(t) \approx \frac{\Delta\varepsilon_{axial}}{\Delta t} = \frac{\varepsilon_{axial}(t_{i+1}) - \varepsilon_{axial}(t_i)}{t_{i+1} - t_i} \quad (13)$$

The calculation of this rate for each time interval within stage VI clearly highlights the acceleration characteristic of tertiary creep. A plot of the axial strain rate versus time for stage VI would exhibit an exponential increase in this rate as the specimen approaches failure (Figure 9).

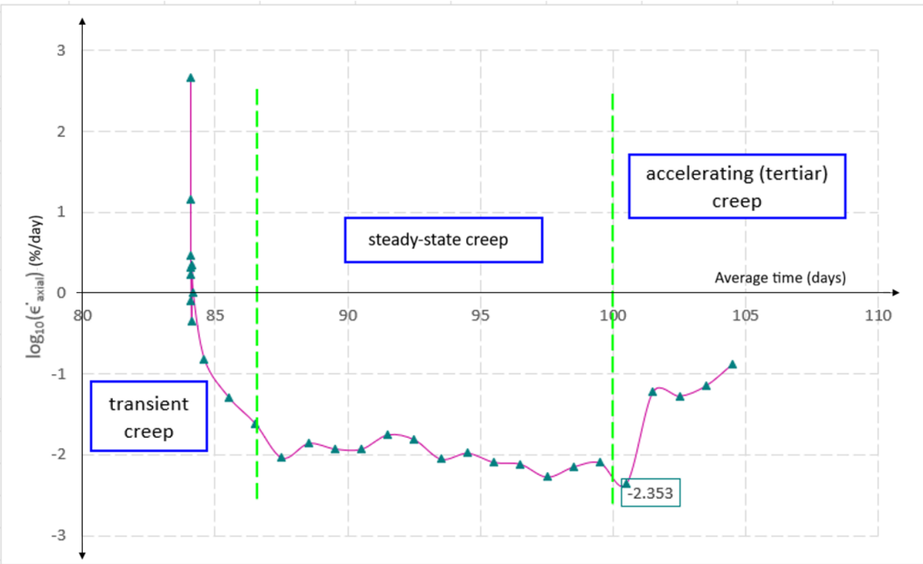

Fig.9. Rheological curve of the axial strain rate: variation of a $lg(\dot{\varepsilon}_{axial})$ as a function of average time ($t_{average}$) highlighting the transition from secondary creep (minimum rate) to tertiary creep (acceleration)

The plot in Figure 9 illustrates the typical evolution of the creep strain rate, representing the three distinct stages of the process for the rock salt tested under maximum stress (stage VI). The logarithmic representation of the rate $lg(\dot{\varepsilon}_{axial}(t))$ allows for a clear visualization of the variations across different orders of magnitude throughout the entire test.

1. Phase I: primary or transient creep: Within the interval between the initial moment and approximately day 87, the material behaviour is characterized by a sharp decrease in the logarithmic rate, from its maximum value toward negative values. This phase reflects a rapid microstructural rearrangement, known as strain hardening (or work hardening), a process occurring under the influence of the applied load. From an internal mechanism perspective, the deformation energy is initially consumed to activate creep mechanisms and to accumulate dislocations; this phenomenon leads to a progressive increase in the material's resistance, thereby resulting in an implicit reduction in the strain rate.

2. Phase II: secondary creep (or steady-state creep): Within the interval between day 87 and day 100, the material behaviour stabilizes, with the curve reaching a quasi-horizontal plateau characteristic of the steady-state creep zone. In this region, the logarithmic rate remains relatively constant, oscillating between $lg(\dot{\varepsilon}_{axial}(t)) \approx -1.75$ and a minimum of -2.353. The minimum rate point is reached at $lg(\dot{\varepsilon}_{min}(t)) = -2.353$ (corresponding to a rate of ≈ 0.0044 %/day) around day 100.5 and represents the steady-state creep rate ($\dot{\varepsilon}_s$) defined by Norton's law. From a mechanical standpoint, this stage reflects a dynamic equilibrium in which the rate of microstructural hardening is offset by the material's recovery or relaxation rate.

The fact that this stage is brief and not perfectly flat suggests either a high sensitivity of the salt to degradation or a rapid transition toward internal damage under the effect of high stress.

3. Phase III: tertiary creep (accelerating creep): After reaching the minimum strain rate around day 100.5, the curve exhibits a rapid and exponential increase, marked by a pronounced positive slope in the logarithmic plot, which confirms the material's transition into the tertiary creep stage. This acceleration is caused by the irreversible damage to the material's microstructure—a process including the nucleation, growth, and coalescence of micro-cracks and voids—and is closely linked to the dilatancy phenomenon observed in the volumetric strain analysis. The increase in the logarithmic rate from -2.353 to a maximum of -0.876 (corresponding to a rate of approximately 0.133%/day) within a short time interval indicates critical rheological instability and the imminence of specimen failure.

The plot provides robust visual evidence that under high stress levels (stage VI), the behaviour of Slănic Prahova rock salt is governed by processes that, despite an initial tendency to stabilize (secondary creep), rapidly succumb to damage mechanisms. The measurement of the minimum creep rate $(lg(\dot{\varepsilon}_{min}(t)) = -2.353$ is a fundamental parameter for calibrating damage-creep viscous-plastic models, which are essential for long-term engineering stability predictions.

4.8. Lifetime estimation (tertiary creep) for the final loading stage

For the final loading stage (stage VI), a clear acceleration in strain was observed, signalling the onset of the tertiary creep stage, which precedes material failure. An estimation of the remaining lifetime was attempted by extrapolating the tertiary creep curve.

Application of exponential extrapolation

Given the evident acceleration, a simple linear extrapolation of the final data points would likely significantly underestimate the remaining lifetime. A more appropriate approach involves fitting an exponential function to the final measurements recorded during stage VI, as this model can accurately describe an accelerated growth pattern:

$$\varepsilon = A \cdot e^{B \cdot t} \tag{14}$$

Through logarithmic transformation, this becomes linear:

$$ln(\varepsilon) = ln(A) + B \cdot t \tag{15}$$

The transformed data used for regression and the linear regression results are presented in Table 6 and Figure 10.

By applying linear regression of *ln(ε)* as a function of B, the slope and the intercept (*ln(A)*), were obtained. Consequently, the exponential model for tertiary creep is expressed as:

$$\varepsilon(t) \approx 0.194 \times e^{0.027 \times t} \tag{16}$$

Table 6. Transformed data values for the exponential model regression

Time (days)	Strain (%)	ln(ε)
102.01	3.027	1.108
103.01	3.081	1.126
104.01	3.152	1.148
105.01	3.285	1.190

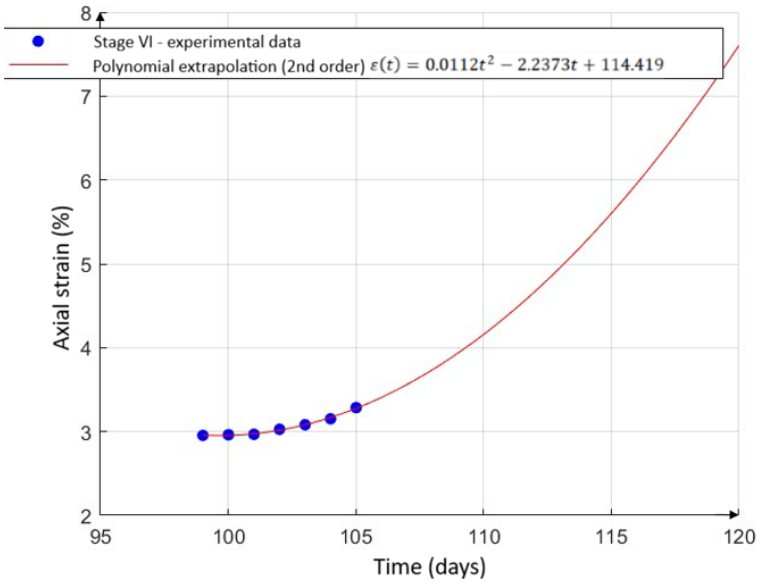

Fig.10. Extrapolation of the tertiary creep curve for stage VI using an exponential model

The exponential extrapolation presented in Figure 10 provides a high-precision mathematical fit for the final stage of deformation (stage VI). The quantitative analysis of this model reveals the following:

Model precision: The regression analysis of the transformed data from Table 6 yields an exceptionally high coefficient of determination, confirming that the exponential function accurately captures the acceleration phase of the rock salt.

Strain acceleration: Between day 102.01 and day 105.01, the axial strain increases from 3.027 % to 3.285 %. This represents a deformation increase of approximately 8.5 % in just 3 days, highlighting the rapid loss of structural integrity as the material approaches failure.

Extrapolation to the 120-day threshold: Following the trajectory defined by the model $\varepsilon(t) = 0.0112t^2 - 2.2373t + 114.419$ (as shown in the figure), the strain is projected to accelerate significantly. While the deformation at 105 days is 3.285%, the curve indicates that the strain will more than double, reaching approximately 7.5% - 8% by day 120.

Predictive value: This quantitative surge validates the decision to use a non-linear model. A simple linear extrapolation would have predicted a strain of only ~4.5 % at 120 days, thereby dangerously underestimating the risk of sudden collapse.

Estimation of time to failure

To estimate the time to failure (t_r), a critical strain value at which material failure occurs must be assumed. In the absence of specific empirical data, estimations are performed based on hypothetical values. For our case, a failure strain of 5 % was considered, resulting in an estimated time to failure of approximately 120.3 days; for a presumed failure strain of 10 %, the estimated time is approximately 146 days. This estimation is highly dependent on the assumed critical failure strain and the validity of the exponential model's extrapolation beyond the available data set. A different failure strain value would lead to a significantly different lifetime estimation.

It must be noted that extrapolation based on a limited number of data points during the tertiary stage can be imprecise. For a more reliable estimation, it would be ideal to have experimental data recorded until actual failure or to utilize a constitutive tertiary creep model specifically designed for rock salt, whose parameters would be fitted to a more extensive experimental data set.

5. Conclusions and limitations

This study experimentally investigated and modelled the viscoplastic behaviour of Slănic Prahova rock salt under multi-stage uniaxial loading, deriving essential constitutive parameters for evaluating the long-term stability of underground structures. The research led to the following conclusions:

1) Creep modelling and dominant mechanisms: The analysis confirmed the presence of all three creep stages (primary, secondary, and tertiary), alongside a complex volumetric behaviour indicating a transition toward dilatancy and structural degradation under high stress levels.

2) Norton model calibration: Modelling the secondary creep using Norton's law yielded a stress exponent $n \approx 1.57$, suggesting that mass transport and diffusion-based mechanisms are dominant in the tested salt.

2) Interpretation of statistical dispersion: The Norton model showed a moderate coefficient of determination ($R^2 \approx 0.58$), a direct result of the non-monotonic behaviour observed at intermediate stress levels. This statistical mismatch indicates that a simple power-law model is insufficient to fully capture the microstructural complexity and the competition between strain hardening and recovery mechanisms.

3) Stability assessment and lifetime estimation: At the highest applied stress (11.76 MPa), an exponential acceleration of strain was observed, characteristic of tertiary creep.

4) Quantitative predictions: Through exponential extrapolation, the remaining lifetime was estimated at approximately 120 days before reaching a critical strain threshold of 5 %. The final axial strain relative to cumulative time is most accurately described by a power-law model ($R^2 \approx 0.868$), providing a robust basis for long-term failure predictions.

5) Engineering implications: From a geomechanical perspective, these results provide essential local rheological parameters, including the long-term strength threshold (), indicating an operational stability timeframe between 7 and 15 years for the analysed salt massif.

Limitations and future work: While Norton's law provides a fundamental basis for identifying diffusion-controlled mechanisms, it cannot fully account for the intricate interplay between structural hardening and microstructural deterioration. To enhance the precision of geomechanical predictions, future research should integrate more advanced rheological frameworks, such as the Burgers or Nishihara models, or constitutive creep-damage formulations capable of capturing the non-monotonic evolution of the strain rate and the effects of internal deterioration

References

[1] **Hammett R.D., Hoek E.,** 1981
Design of Large Underground Caverns for Hydroelectric Projects, with Reference to Structurally Controlled Failure Mechanisms. Proc. American Soc. Civil Engrs. Int. Conf. on recent developments in geotechnical engineering for hydro projects. 192-206. New York: ASCE

[2] **Zhang G., Wu Y., Wang L., Zhang K., Daemen J. J. K., Liu W.,** 2015
Time-Dependent Subsidence Prediction Model and Influence Factor Analysis for Underground Gas Storages in Bedded Salt Formations. Engineering Geology, vol. 187, pp. 156–169

[3] **Ma L.J., Xu H.F., Wang M.Y., Li E.B.,** 2015
Numerical Study of Gas Storage Stability in Bedded Rock Salt during the Complete Process of Operating Pressure Runaway. Chinese Journal of Rock Mechanics and Engineering, vol. 34, no. S2, pp. 4108–4115

[4] **Sun J.,** 2007
Rock Rheological Mechanics and Its Advance in Engineering Applications. Chinese Journal of Rock Mechanics and Engineering, vol. 26, no. 6, pp. 1081–1106

[5] **Zhou Z.W., Liu J.F., Wu F. et al.,** 2016
Experimental Study on Creep Properties of Salt Rock and Mudstone from Bedded Salt Rock Gas Storage. Journal of Sichuan University (Engineering Science Edition), vol. 48, no. S1, pp. 100–106

[6] **Singh A., Kumar C., Kannan L.G., Rao K.S., Ayothiraman R.,** 2017
Rheological Behaviour of Rock Salt under Uniaxial Compression. Procedia Engineering 173 (2017) 639-646.

[7] **Carter N.L., Horseman S.T., Russell J.E., Handin L.,** 1993
Rheology of Rocksalt. Journal of Structure Geology, vol. 15, no. 9-10, pp. 1257–1271

[8] **Langer M.,** 1981
The Rheological Behaviour of Rock Salt. In: The Mechanical Behaviour of Salt, Proc. of the First Conf., University Park (USA) 1981; Editors: Hardy, H. R. Jr. & M. Langer; p. 201–240. Trans Tech Publ., Clausthal

[9] **Fan J., Tang L., Fourmeau M., Li Z., Liu W., Zou Y., Jiang D.,** 2025
A Novel Viscoplastic Model for Salt Rock Deformation under Internal Cyclic Gas Pressure Loading, International Journal of Mining Science and Technology, Volume 35, Issue 6, 2025, Pages 989-1004, ISSN 2095-2686, https://doi.org/10.1016/j.ijmst.2025.05.005

[10] **Yang C., Daemen J.J.K., Yin J.-H.,** 1999
Experimental Investigation of Creep Behaviour of Salt Rock. International Journal of Rock Mechanics and Mining Sciences, vol. 36, no. 2, pp. 233–242

[11] **Liang X., Feng G., Meng T., Zhao G., Wang Z., Liu P., Taherdangkoo R.,** 2024
Non-Constant Evolution of Mixed Mode Fracture Process Zone in Heat-Treated Salt Rock during the Whole Loading, Theoretical and Applied Fracture Mechanics, Volume 130, 2024, 104337, ISSN 0167-8442, https://doi.org/10.1016/j.tafmec.2024.104337

[12] **Yang F., Fan J., Yang Z., Liu W., Chen J.,** 2023
Plasticity Analysis and Constitutive Model of Salt Rock under Different Loading Speeds, Journal of Energy Storage, Volume 67, 2023, 107583, ISSN 2352-152X, https://doi.org/10.1016/j.est.2023.107583

[13] **Jin J., Cristescu N.D.,** 1998
An Elastic/ Viscoplastic Model for Transient Creep of Rock Salt. International Journal of Plasticity, vol. 14, no. 1–3, pp. 85–107

[14] **Yanlin Z., Xiaguang W., Wenyu T., Yang L., Hang L., Yixian W., Lianyang Z.,** 2023
Creep Behaviour of Layered Salt Rock under Triaxial Loading and Unloading Cycles. Applied Rheology, vol. 33, no. 1, 2023, pp. 20230103. https://doi.org/10.1515/arh-2023-0103

[15] **Wang R., Jiang Y., Yang C., Huang F., Wang Y.,** 2018
A Nonlinear Creep Damage Model of Layered Rock under Unloading Condition. Mathematical Problems in Engineering, vol. 2018, Article ID 8294390, pp. 1–8

[16] **Zhou T., Qin Y., Ma Q.,** 2020
Exploration of Continuous Rheological Model for Rock under Uniaxial Compression Based on Phenomenological Damage Theory. AIP Advances 10, 105218 (2020). https://doi.org/10.1063/5.0026650

[17] **Li Z., Nguyen T.S., Su G., Labrie D., Barnichon J.D.,** 2017
Development of a Viscoelastoplastic Model for a Bedded Argillaceous Rock from Laboratory Triaxial Tests. Can. Geotech. J. 54: 359–372 (2017) dx.doi.org/10.1139/cgj-2016-0100

[18] **Hunsche U.,** 1991
Volume Change and Energy Dissipation in Rock Salt during Triaxial Failure Tests. In: Cocks, A.C.F., Ponter, A.R.S. (eds) Mechanics of Creep Brittle Materials 2. Springer, Dordrecht. https://doi.org/10.1007/978-94-011-3688-4_15

[19] **Alkan H., Cinar Y., Pusch G.,** 2007
Rock Salt Dilatancy Boundary from Combined Acoustic Emission and Triaxial Compression Tests. International Journal Rock Mechanics and Mining Science, 44 (1)

[20] **Zhang H., Wang Z., Zheng Y., Duan P., Ding S.,** 2012
Study on Triaxial Creep Experiment and Constitutive Relation of Different Rock Salt. Safety Science, vol. 50, no. 4, pp. 801–805

[21] **Cristescu N., Hunsche U.,** 1991
A Constitutive Equation for Salt. Paper presented at the 7th ISRM Congress, Aachen, Germany, September 1991

[22] **Escanellas A., Cámara E., Liaudat J., Carol I.,** 2025
Experimental Study of the Time-Dependent Behaviour of Fracture Propagation in Salt Rock, Geomechanics for Energy and the Environment, Volume 43, 2025, 100687, ISSN 2352-3808, https://doi.org/10.1016/j.gete.2025.100687

[23] **Kolano M., Cała M., Stopkowicz A.,** 2024
Mechanical Properties of Rock Salt from the Kłodawa Salt Dome-A Statistical Analysis of Geomechanical Data. Materials (Basel). 2024 Jul 18;17(14):3564. doi: 10.3390/ma17143564. PMID: 39063857; PMCID: PMC11279227

[24] **Fan J., Li Z., Yang C., Wang T.,** 2025
Creep–Fatigue Mechanical Characterization of Rock Salt under Uniaxial Stresses. In: Investigation in the Creep-Fatigue Coupled Effect of Rock Salt. Springer, Singapore. https://doi.org/10.1007/978-981-96-5431-4_5

[25] **Song Z., Konietzky H., Wu Y., Du K., Cai X.,** 2022
Mechanical Behaviour of Medium-Grained Sandstones Exposed to Differential Cyclic Loading with Distinct Loading and Unloading Rates, Journal of Rock Mechanics and Geotechnical Engineering, Volume 14, Issue 6, 2022, Pages 1849-1871, ISSN 1674-7755, https://doi.org/10.1016/j.jrmge.2021.12.027

[26] **Blanco-Martín L., Azabou M., Rouabhi A., Hassen F.H.,** 2023
Laboratory Experiments on Rock Salt and Phenomenological Observations. International Journal of Rock Mechanics and Mining Sciences, 2023, 170, pp.105452. 10.1016/j.ijrmms.2023.105452. hal-04142503

[27] **Xi B.P., Zhao Y.S., Zhao J.C., Xu S.G.,** 2008
Study on Coupled Thermo-Mechanical Creep Properties of Bedded Rock Salt. Chinese Journal of Rock Mechanics and Engineering, vol. 27, no. 1, pp. 90–96

[28] **Wang M., Li X.G., Yang C.H., Huang Z.Q.,** 2010
Study of Interaction between Creep Deformation of Bedded Salt Rock. Rock and Soil Mechanics, vol. 31, no. 12, pp. 3964–3970

[29] **Zhao Y.L., Zhang Y., Wan W.,** 2010
Mechanical Properties of Bedded Rock Salt and Creep Failure Model. Mineral Engineering Research, vol. 25, no. 1, pp. 16–20

[30] **Huang X.L., Yang C.H., Li Y.P.,** 2014
Interface Shear Stress Distribution of Bedded Salt Rock Considering Rheology Effect. Chinese Journal Underground Space Engineering, vol. 10, no. 3, pp. 547–551

[31] **Xing W., Zhao J., Düsterloh U. et al.,** 2014
Experimental Study of Mechanical and Hydraulic Properties of Bedded Rock Salt from the Jintan Location. Acta Geotechnica, vol. 9, no. 1, pp. 145–151

[32] **Toderas M., Danciu C.,** 2025
An Investigation into the Creep Behaviour of Rock Salt from Slanic Prahova. Book chapter in Engineering Research: Perspectives on Recent Advances, Vol. 2, 22 January 2025, Page 31-82. DOI: https://doi.org/10.9734/bpi/erpra/v2/3891 https://stm.bookpi.org/ERPRA-V2/article/view/16912

[33] **Li Shi-Y., Urai J.L.,** 2016
Rheology of Rock Salt for Salt Tectonics Modelling. Springer, Pet. Sci. (2016) 13:712–724. DOI 10.1007/s12182-016-0121-6

[34] **Griggs D.,** 1939
Creep of Rocks. The Journal of Geology, vol. 47, no. 3, pp. 225–251

[34] **Stamatiu M.,** 1959
Problema dimensionării stâlpilor la minele de sare din R.P.R. București: Academia Republicii Populare Române

[36] **Stamatiu M.,** 1964
Mecanica rocilor. București: Ed. Didactică și Pedagogică

[37] **Cristescu N.D., Hunsche U.,** 1998
Time Effects in Rock Mechanics. New York, NY, John Wiley and Sons, pp. 343

[38] **Jin J., Cristescu N. D.,** 1998
An Elastic/Viscoplastic Model for Transient Creep of Rock Salt. International Journal of Plasticity, vol. 14, no. 1–3, pp. 85–107

[39] **Cao W.G., Chen K., Tan X., Chen H.,** 2020
A Novel Damage-Based Creep Model Considering the Complete Creep Process and Multiple Stress Levels. Computer and Geotechnics, vol. 124, Article ID 103599

[40] **Wang X., Song L., Xia C., Han G., Zhu Z.,** 2021
Nonlinear Elasto-Visco-Plastic Creep Behaviour and New Creep Damage Model of Dolomitic Limestone Subjected to Cyclic Incremental Loading and Unloading. Sustainability 2021, 13, 12376. https://doi.org/10.3390/su132212376

[41] **Toderaș M., Militaru Șt.,** 2023
Rheological Characteristics of the Rock Salt from Slanic Prahova, Horizon XIV Below Level of 200 m. Mining Revue, vol.29, no.3, 2023, pp.26-43. https://doi.org/10.2478/minrv-2023-0021

[42] **Klepaczko J.R., Gary G., Barberis P.,** 1991
Behaviour of Rock Salt in Uniaxial Compression at Medium and High Strain Rates. Arch. Mech. 43, 4. Pp. 499-517. Warszawa

[43] **Chen J., Shi X., Zhou J.,** 2016
The Mechanical Characteristic of Rock Salt under Uniaxial Compression with Low Temperature Effect. Functional Materials, 23, No.3 (2016), p. 433-436. ISSN 1027-5495. http://dx.doi.org/10.15407/fm23.03.433

[44] **Fan J., Yang F., Li Z., Zou Y., Chen J., Jiang D., Nelias D.,** 2025
Creep Constitutive Model for Salt Rock Considering Loading and Unloading Path Based on State Variables. Geomech. Geophys. Geo-energ. Geo-resour. (2025) 11:30. https://doi.org/10.1007/s40948-025-00944-4